Integrated Assembly and Photopreservation of Topographical Micropatterns

Shuailong Zhang, Weizhen Li, Mohamed Elsayed, Jiaxi Peng, Yujie Chen, Yanfeng Zhang, Yibo Zhang, Moein Shayegannia, Wenkun Dou, Tiancong Wang, Yu Sun, Nazir P. Kherani, Steven L. Neale, and Aaron R. Wheeler*

Micromanipulation techniques that are capable of assembling nano/micro-materials into usable structures such as topographical micropatterns (TMPs) have proliferated rapidly in recent years, holding great promise in building artificial electronic and photonic microstructures. Here, a method is reported for forming TMPs based on optoelectronic tweezers in either "bottom-up" or "top-down" modes, combined with in situ photopolymerization to form permanent structures. This work demonstrates that the assembled/cured TMPs can be harvested and transferred to alternate substrates, and illustrates that how permanent conductive traces and capacitive circuits can be formed, paving the way toward applications in microelectronics. The integrated, optical assembly/preservation method described here is accessible, versatile, and applicable for a wide range of materials and structures, suggesting utility for myriad microassembly and microfabrication applications in the future.

1. Introduction

Microassembly technologies have proliferated in recent years, driven by great interest in the capacity to manufacture functional micro- and nanodevices for a wide range of applications. Most of these microassembly technologies rely on "pick-and-place" techniques,[1–8] in which a robotic arm with a "catch-and-release" tip is used to mechanically select targeted objects to assemble them into desired combinations and geometries, which we call "topographical micropatterns" (TMPs). These assembly techniques are useful, but they also rely on expensive and specialized positioning tools and well-trained personnel, and can be limited by material properties and throughput.

Optical assembly is an alternative strategy to assemble functional structures from micro- and nano-objects as building blocks.[9] Optical assembly relies on optical micromanipulation technologies such as optical tweezers,[9–13] opto-thermophoretic tweezers,[14–16] photovoltaic tweezers,[17–20] and optoelectronic tweezers,[21–30] in which micro- and nano-objects are optically assembled into a pattern in a fluidic environment and later dried for use in various applications. This approach has advanced rapidly in recent years, and preserves many of the advantages of the conventional methods while being easy-to-implement and allowing for cost-effective operation. Among different optical micromanipulation techniques, optoelectronic tweezers (OET) has proven to be particularly useful for the assembly of large numbers of micro- and nano-objects in parallel,[22–31] and also for the assembly of micro-objects with "large" sizes (with at least one dimension greater than 150 μm).[32–34] However, one limitation for OET assembly (and also for other optical assembly techniques)

S. Zhang,[+],[++] M. Elsayed, J. Peng, A. R. Wheeler
Donnelly Centre for Cellular and Biomolecular Research
University of Toronto
Toronto, ON M5S 3E1, Canada
E-mail: aaron.wheeler@utoronto.ca

S. Zhang, J. Peng, A. R. Wheeler
Department of Chemistry
University of Toronto
Toronto, ON M5S 3H6, Canada

S. Zhang, M. Elsayed, J. Peng, Y. Sun, A. R. Wheeler
Institute of Biomedical Engineering
University of Toronto
Toronto, ON M5S 3G9, Canada

iD The ORCID identification number(s) for the author(s) of this article can be found under https://doi.org/10.1002/smll.202103702.

[+]Present address: Beijing Advanced Innovation Center for Intelligent Robots and Systems, Beijing Institute of Technology, Beijing, 100081, China
[++]Present address: School of Mechatronical Engineering, Beijing Institute of Technology, Beijing, 100081, China

W. Li, S. L. Neale
James Watt School of Engineering
University of Glasgow
Glasgow G12 8LT, UK

Y. Chen, Y. Zhang
State Key Laboratory of Optoelectronic Materials and Technologies
School of Electronics and Information Technology
Sun Yat-sen University
Guangzhou 510275, China

Y. Zhang, M. Shayegannia, Y. Sun, N. P. Kherani
Department of Electrical and Computer Engineering
University of Toronto
Toronto, ON M5S 3G4, Canada

W. Dou, T. Wang, Y. Sun
Department of Mechanical and Industrial Engineering
University of Toronto
Toronto M5S 3G8, Canada

N. P. Kherani
Department of Materials Science and Engineering
University of Toronto
Toronto, ON M5S 3E4, Canada

is that the process must be performed in a fluidic environment, such that the fluid must be removed afterward, often by evaporation, a chaotic process that can destroy the structure that has (up to that point) been carefully assembled. This problem is partly solved via a previously reported freeze-drying process, in which the liquid medium is frozen and then sublimated.[29,35] However, the freeze-drying process requires that the assembled structure be compatible with low temperatures and low pressures, which sets limitations on the materials that can be used. In addition, freeze-drying increases the time of operation and the system complexity.

Here, we report a new method of TMP assembly, using OET to assemble micro- and nano-objects into functional structures that are then preserved via in situ photopolymerization. This technique is enabled by a digital micromirror device (DMD) integrated with independently controlled light sources with different wavelengths, which can be used to both assemble the nano/micro-objects and to preserve their structures via selective photopolymerization of a hydrogel solution. In this introductory report, we demonstrate that carbon/silver nanoparticles, graphene nanoplatelets and polystyrene microbeads can be assembled into TMPs in either a "bottom-up" mode, in which up to hundreds of thousands of particles are brought together in parallel (analogous to structural self-assembly) or a "top-down" mode, in which particles are manipulated one-by-one (analogous to pick-and-place assembly). After formation, the TMPs are immobilized/preserved via photopolymerization and

can be transferred onto a variety of flexible and rigid substrates. Most uniquely, we demonstrate how metallic microspheres can be assembled to form permanent conductive electrical traces and to assemble capacitors into working microcircuits. We propose that the new method presented here is versatile and powerful, and could be useful for a wide range of microassembly and microfabrication applications in the future.

2. Results and Discussion

The methods introduced here rely on OET, a technique that utilizes light-induced dielectrophoresis (DEP) to manipulate nano/micro-objects.[21,36] Similar to our previous reports,[34,37] the OET devices used here consist of two plates formed from indium tin oxide (ITO)-coated glass slides. The bottom plate was coated with an additional layer of photoconductive material—hydrogenated amorphous silicon (a-Si:H). The devices were assembled by adhering the top and bottom plates together with a spacer to form a chamber, within which the manipulation was performed by projecting patterns of light onto the a-Si:H layer to form locally conductive "virtual electrodes" to drive DEP. In a departure from previous OET work, the system was configured to allow the DMD to control different wavelengths (including red light from a 620 nm diode and UV light from a 380 nm diode), as shown in **Figure 1**a. The different wavelengths of light
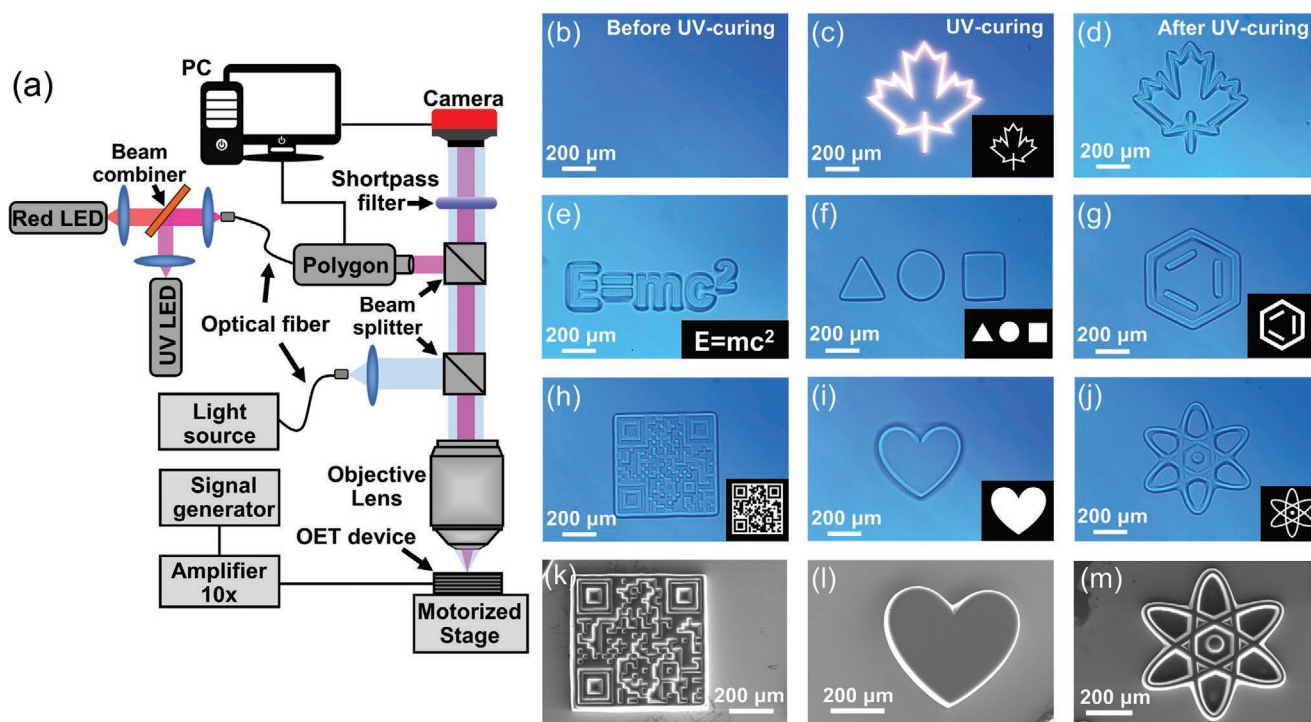

Figure 1. Experimental setup and polymerized hydrogel structures. a) Schematic of the experimental setup, featuring LEDs with two wavelengths (red: 620 nm; UV: 380 nm) that can be controlled by a Polygon DMD (Mightex Inc.). b–d) Bright-field microscope images (frames from Movie S1 in the Supporting Information) demonstrating the UV photopolymerization process of sol-form hydrogel solution (concentrated PEGDA) to form a 3D microstructure of an outline of a "maple leaf." Bright-field microscope images (many from frames of Movie S1 in the Supporting Information) of cured hydrogel microstructures in the form of e) the mass–energy equation, f) a triangle, circle, and square, g) the chemical symbol for benzene, h) a quick response (QR) code, i) a "heart" symbol, and j) an "atom" symbol. The insets are the black and white images that were projected into the device to generate the cured hydrogel microstructures. Representative SEM images of cured hydrogel microstructures, showing the k) QR code, l) "heart" symbol, and m) "atom" symbol.

**ADVANCED
SCIENCE NEWS**
www.advancedsciencenews.com

**NANO · MICRO
small**
www.small-journal.com

are focused through the objective of an upright microscope to form light patterns on the photoconductive substrate in the OET device. In this technique, the chamber of the OET device contains both the nano/micro-objects to be manipulated as well as a sol-form of a photopolymerizable poly(ethylene glycol) diacrylate (PEGDA) hydrogel solution. When red light is projected into the OET device and an AC bias is applied, the device operates in OET mode, in which nano/micro-objects are manipulated and assembled, and when UV light is projected into the device, the system operates in "gel-curing" mode, in which the hydrogel solution is polymerized. After the polymerization, a solid structure is formed and the assembled nano/microstructures are immobilized and encapsulated in the solid structure.

We are aware of three previous reports describing the use of OET,[38] optical tweezers,[39] or opto-thermophoretic tweezers[40] to assemble particles into microstructures that were subsequently immobilized by photopolymerization. Two of these methods[39–40] were limited to "top-down" assembly of structures from fewer than 10 particles, and in all of them, the photopolymer did not have a particular structure—it was just a shapeless "carrier" used to immobilize the assembled particles. Here, we introduce a new strategy in which the photopolymer is also formed into defined shapes, making use of the same DMD which is used to control the OET/DEP forces (see below), to enhance the ultimate utility of the finished products. Movie S1 in the Supporting Information (clip 1) and Figure 1b–d illustrate the process of forming a photopolymerized structure—in this case, a 3D outline of a "maple leaf." As shown, when the appropriate pattern is projected into the device, the prepolymer solution becomes cross-linked (only in regions exposed to UV light), and the solid structures become cured in around 5 s, after which the remaining prepolymer solution can be rinsed away. Using the DMD allows for straightforward generation of photopolymerized structures with controllable geometries, selected on demand. For example, Movie S1 in the Supporting Information (clips 2–6) and Figure 1e–j show examples of different geometries (cartoons, numbers, letters, symbols and shapes) that can be formed. As described in the supplementary information file (and as illustrated in Figure S1 in the Supporting Information), the process is straightforward with a user-friendly computer interface, making this technique easy to teach to new users. After forming the microstructures, they can subsequently be extracted and used for a variety of applications; for example, scanning electron microscope (SEM) images of three of the structures are shown in Figure 1k–m. Although the DMD projection-photopolymerization method described here has poorer resolution than that of other maskless lithography techniques such as two-photon polymerization[41] and dip-pen lithography,[42] it offers a number of advantages, including relatively high throughput, user-friendly operation, and compatibility with enclosed systems. Note that the height of polymerized structures in the current system is defined by the chamber dimensions; in the future, more precise Z-axis control might be possible by integration with two-photon techniques.[41]

The concentrated PEGDA solution used to form the structures in Figure 1 has high viscosity, which hampers manipulation of particles suspended in that solution by OET. To identify conditions that allow both UV-curing and OET manipulation, dilutions of concentrated PEGDA solution in DI water were formed (1:1, 1:2, 1:3, 1:4, and 1:5), and each was tested and evaluated based on the performance of OET manipulation and UV curing. Movie S2 in the Supporting Information and **Figure 2**a,b illustrate a typical OET manipulation experiment: a doughnut-shaped light pattern (red) is projected into a sol-form PEGDA solution to move a 10 µm diameter polystyrene microbead. In these experiments, the OET device was driven at an AC bias of 15 V_{pp} at 20 kHz, which generated a negative DEP force that caused the particle to remain within the dark region of the doughnut (in cases in which the DEP force was greater than viscous drag). The maximum moving velocities as well as the percentage of movable polystyrene microbeads were measured in different dilutions of concentrated PEGDA to DI water. As shown in Figure 2c, both properties increase as PEGDA concentration decreases, likely because of reduced viscosity.

Each PEGDA dilution was also evaluated for curing properties when exposed to UV light. For example, Figure 2d–g show bright-field microscopy images of the illumination of different PEGDA solutions with a rectangular- UV light pattern. As shown in Figure 2h, the percentage of the cured area (compared to the area of the UV light pattern) decreases with a decreasing ratio of concentrated PEGDA, and the time required for the solution to cure increases with a decreasing ratio of concentrated PEGDA. Therefore, a trade-off exists between OET particle manipulation performance and UV curing performance when choosing the dilution of concentrated PEGDA. Based on the results in Figure 2c,h, a ratio of 1:4 concentrated PEGDA solution to DI water was selected to ensure both effective particle manipulation and UV photopolymerization. This ratio was used for all of the experiments described below.

After determining an optimum ratio of concentrated PEGDA to DI water in the solution, experiments were carried out to explore the capacity to assemble up to hundreds of thousands of nano/microparticles into TMPs in bottom-up mode followed by preserving them in cured hydrogel structures. **Figure 3**a illustrates the step-by-step procedure of using red and UV light patterns to assemble nano/micromaterials into TMPs and preserve the assembled TMPs via photopolymerization. (Note that this example illustrates particles that are conductive and experience positive DEP force, drawing the particles into the illuminated region.) Figure 3b–f shows representative microscope images of each step of this process for a suspension of carbon nanoparticles (which experience positive DEP) (Figure 3b) being assembled into a TMP depicting the differential form of one of the Maxwell equations, Gauss's law for magnetism (Figure 3c,d), and then being preserved in a cured hydrogel (Figure 3e,f). Note that the TMP remains unchanged during the photopolymerization, suggesting that potentially disruptive forces caused by UV curing have little influence on the assembled TMP. In general, as illustrated in Movie S3 (Supporting Information), TMPs formed in this "bottom-up" manner feature up to hundreds of thousands of particles that are simultaneously assembled, in a process that requires approx. 40 s of red light projection and approx. 50 s of UV light projection. We have used carbon nanoparticles (Figure 3g,h), silver nanoparticles (Figure 3i,j), and graphene nanoplatelets (Figure 3k,l) (all of which experience positive DEP) to form TMPs representing an assortment of Maxwell's equations, cartoons and chemical formulas, and stylized caricatures of famous scientists. TMPs can
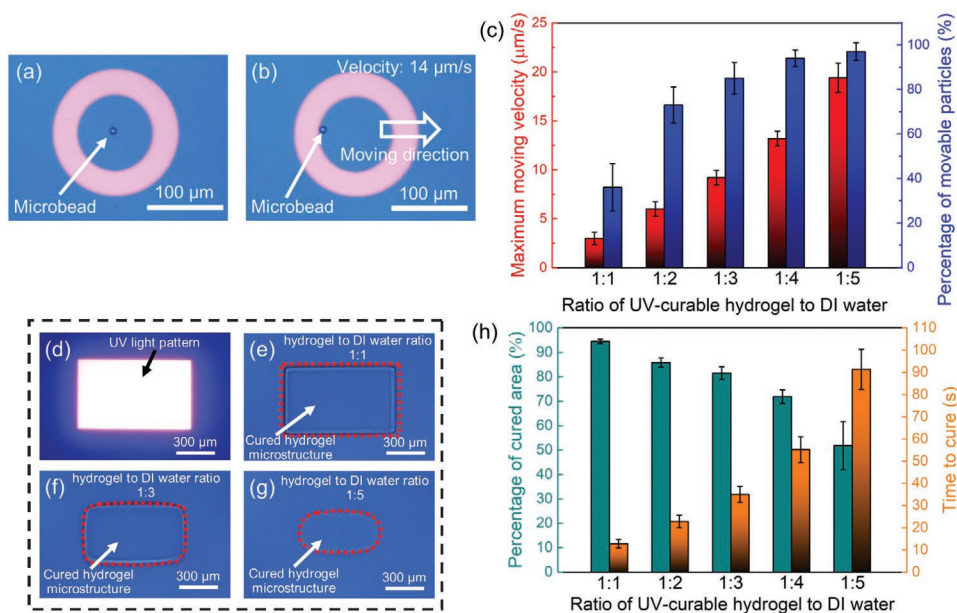
Figure 2. OET particle movement and UV-curable hydrogel curing. Bright-field microscope images (frames from Movie S2 in the Supporting Information) of a) trapping a 10 µm dia. polystyrene microbead and b) moving the bead at 14 µm s^{-1} using a doughnut-shaped light pattern. The white arrow indicates the direction of movement. c) Plots of maximum moving velocity (left, red) and the percentage of movable polystyrene particles (right, blue) in solutions with different dilutions of concentrated PEGDA solution in DI water. Error bars represent standard deviation for five replicates. Bright-field microscope images illustrating the results of projecting a rectangular-shaped UV light pattern d) to cure solutions with 1:1 e), 1:3 f), and 1:5 g) dilutions of concentrated PEGDA solution in DI water. The boundaries of the cured materials in (e)–(g) are highlighted with red dotted outlines. h) Plots of the percentage of cured hydrogel (left, teal, from areas measured relative to the projected UV light pattern) and the required curing time (right, orange) in solutions with different dilutions of concentrated PEGDA solution in DI water. Error bars represent standard deviation for five replicates.

also be formed from dielectric particles that experience negative DEP (via negative red-light patterns), such as polystyrene beads (Figure 3m–o), which (in this example) happen to be fluorescent (Figure 3p). The design possibilities are nearly endless, with additional examples of TMPs found in Figure S2 (Supporting Information), and can be formed from diverse micro/nano materials with a wide range of sizes and shapes, as shown in the SEM images in Figure S3 (Supporting Information).

After demonstrating the capability for (i) assembling TMPs with different designs and different materials using OET, and (ii) immobilizing/preserving the assembled TMPs via UV photopolymerization, we investigated the feasibility of transferring the assembled/cured TMPs in hydrogel microstructures to other substrates. We adapted a technique described previously for moving freeze-dried structures,[29] in which two destination-substrates were used for transfer: polydimethylsiloxane (PDMS) and double-sided adhesive tape. A schematic illustrating the process of transferring assembled/cured TMPs in hydrogel microstructures to the two kinds of substrates is shown in **Figure 4**a. Images illustrating various stages of transfer for both kinds of substrate are shown in Figure 4b–h. During the transfer process, the PDMS substrate functions as an elastomeric stamp which attracts the cured hydrogel microstructures (bearing encapsulated TMPs) by kinetic adhesion;[2] likewise, the chemical adhesive on the double-sided tape allows for capture of cured hydrogel microstructures (with encapsulated TMPs). The transferred hydrogel microstructures and the encapsulated TMPs are robust, such that they can withstand touching and bending. These results

demonstrate proof of concept for the harvest and transfer of TMPs to other acceptor substrates/surfaces, with the potential to serve as anti-counterfeiting markers for official documentation,[29] novelty micrologos for exhibitions or conferences, or (in combination with educational materials related to the principles of DEP and OET and Movie S3 in the Supporting Information) as activities and support for classroom/laboratory instruction.[43] Importantly, none of the previous reports describing photocured TMPs[38–40] described the capacity to transfer the structures after photopolymerization or to use them in any way. We anticipate that this may be possible for these techniques in the future, and this was a key goal in the method described here.

As a test case for using TMPs formed by the techniques described here, we decided to evaluate the potential for forming working microelectronic circuits. As a first step toward this goal, we evaluated the capacity to manipulate conductive Sn$_{62}$Pb$_{36}$Ag$_2$ solder beads, which have spherical structures with sizes ranging from 15 to 25 µm. Like carbon nanoparticles, silver nanoparticles, and graphene nanoplatelets, the solder beads used here experience a positive DEP force. Based on Stokes' law, the viscous drag force F_{Drag} of a trapped particle can be calculated, which can be used to estimate the DEP force F_{DEP} that the particle experiences

$$F_{DEP} = F_{Drag} = 6\pi\eta r v \tag{1}$$

where η is the viscosity of the solution, r is the radius of the solder bead and v is velocity of the particle. Movie S4 in the
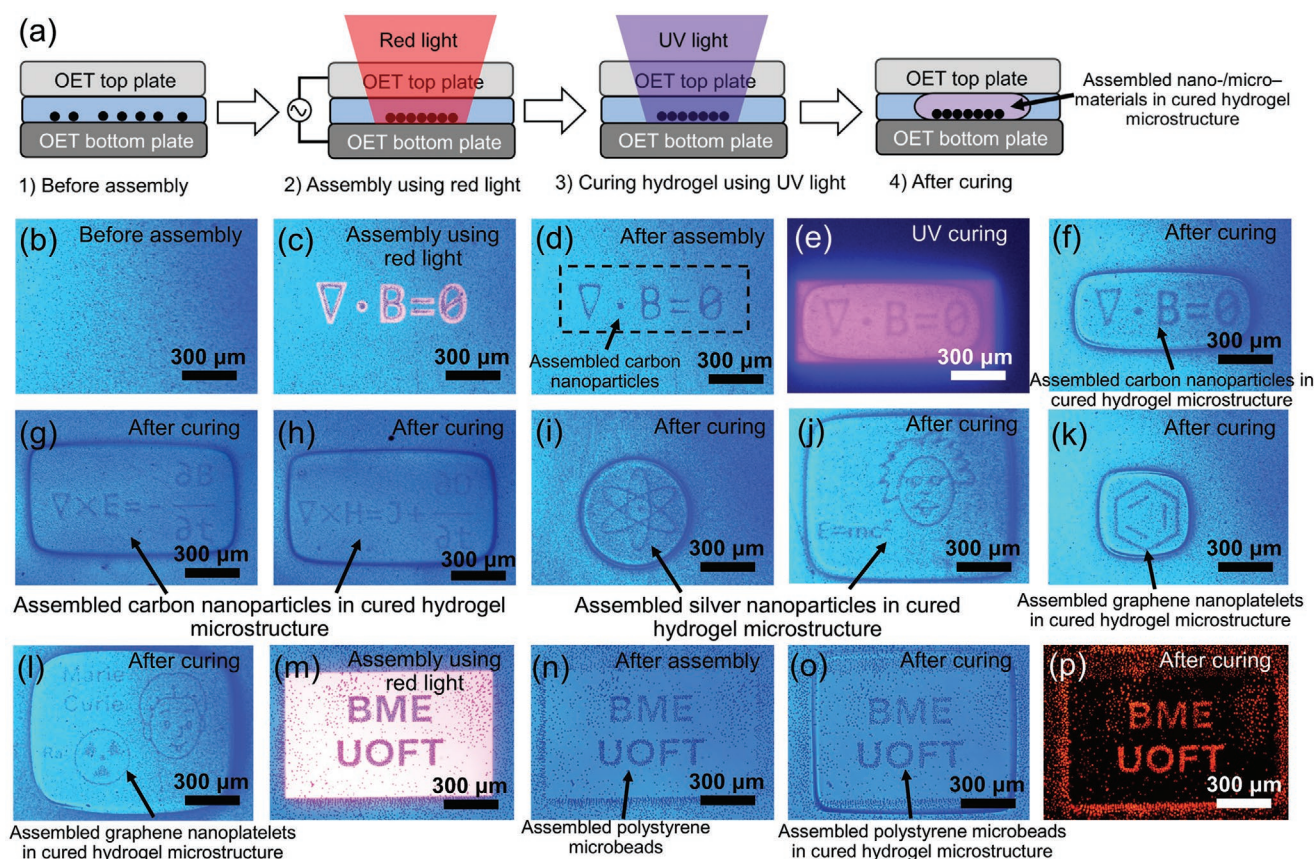
Figure 3. Assembly of nano/micromaterials into TMPs in bottom-up mode and preservation of the assembled TMPs via UV photopolymerization in concentrated PEGDA diluted 1:4 in DI water. a) Schematic process of OET assembly via red light and solution curing via UV light. Bright-field microscopy images of carbon nanoparticles b) before OET assembly, c) during OET assembly d) after OET assembly, e) during UV curing, and f) after UV curing of a TMP featuring the differential form of Gauss's law for magnetism. Bright-field microscopy images of assembled/cured carbon nanoparticle TMPs featuring g) the differential form of Faraday's law and h) the differential form of the Ampere–Maxwell law, assembled/cured silver nanoparticle TMPs depicting i) the "atom" symbol and j) a stylized caricature of Albert Einstein with the mass energy equation, and assembled/cured graphene nanoplatelet TMPs depicting k) the chemical symbol for benzene and l) a stylized caricature of Marie Curie with the symbol for radioactivity. Bright-field microscopy images of 6 μm diameter fluorescent polystyrene microbeads m) during OET assembly, n) after OET assembly, and o) after UV curing of a TMP featuring the text "BME UOFT" (abbreviation for biomedical engineering at the University of Toronto). p) Fluorescence microscopy image of the assembled/cured TMP formed in (m)–(o).

Supporting Information and **Figure 5**a,b illustrate the translation of a 20 μm diameter solder bead using a circular light pattern at 20 and 60 μm s^{-1}. As shown, the center-to-center distance (D in Figure 5a,b) between the bead and the light pattern increases with an increasing velocity and F_{Drag}. By measuring the center-to-center distance at varying velocities, a profile of the DEP force experienced by a bead at different positions within the trap can be plotted, as shown by the markers in Figure 5c. We also investigated the achievable positioning accuracy,[47] which is important for assembly applications. Solder beads were repeatedly translated to randomized destinations between 30 and 500 μm away from their initial positions, and the difference between each bead's relative position in the trap before and after moving, the "post-translational offset" (PTO), was recorded. The PTOs observed for 18 different beads are shown in Figure 5d, with average absolute X- and Y-values found to be 0.71 and 0.69 μm, respectively. Thus, this method, which relies on a 30 μm diameter OET trap, allows for sub-micrometer positioning accuracy.

To further analyze the performance of OET manipulation of the solder bead, the trap profile was simulated in COMSOL Multiphysics based on a 3D model (Figure S4, Supporting Information). Simulated profiles of electric potential and field are shown in Figure 5e,f. As indicated, these properties (an in particular the field) vary substantially across the solder bead, which renders inappropriate the assumption (that is often made in DEP simulations) that the field is invariant with respect to the trapped particle. Thus, a numerical estimate of DEP force on the particle F_{DEP} was generated by integrating the Maxwell stress tensor over the surface of the bead, a method described previously[48,49] for approximating behavior in systems in which a trapped particle causes substantial perturbation to the applied electric field. Details of the simulation are in the supplementary information file, and as shown by the red plot in Figure 5c, the result has good qualitative agreement with experimental observations.

After clarifying the trap profile and the accuracy for the positioning of solder beads in the OET system, we explored the
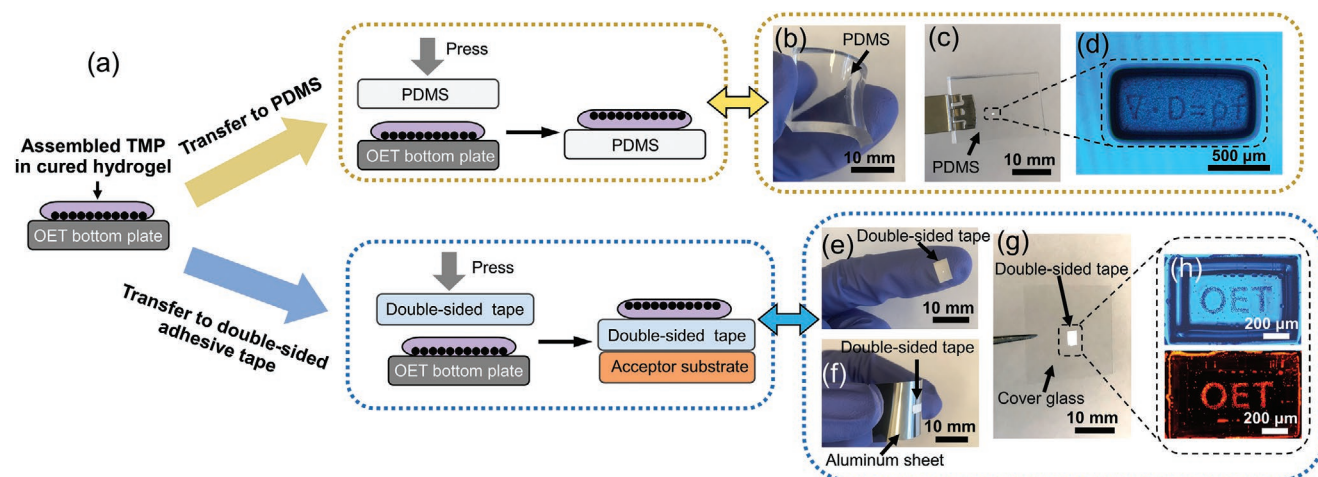
**ADVANCED
SCIENCE NEWS**

www.advancedsciencenews.com

NANO · MICRO

small

www.small-journal.com

Figure 4. Transfer of assembled/cured TMPs to destination substrates. a) Schematic illustration of transferring TMPs encapsulated in cured hydrogel microstructures (formed in concentrated PEGDA diluted 1:4 in DI water) to PDMS (grey, in yellow-dashed box), and double-sided adhesive tape (blue, in blue-dashed box) substrates. The latter (double-sided tape) is then mounted on an acceptor substrate (orange). b,c) Images of PDMS substrates bearing assembled, cured, and transferred TMPs. d) Microscope image of a TMP depicting the differential form of Gauss's law for electric fields in a cured hydrogel microstructure after transfer to a PDMS substrate. Images of double-sided tape substrates bearing assembled/cured TMPs mounted on e) a glove, f) a flexible aluminum sheet, and g) a cover glass. h) Bright-field (top) and fluorescence (bottom) microscopy images of cured/assembled TMP featuring the text "OET" (abbreviation for optoelectronic tweezers) after transfer to a double-sided tape substrate.

capacity for top-down assembly of solder beads to form conductive traces to bridge isolated electrodes, a common proof of concept used to evaluate electronic assembly/construction.[50–52]

As described in the supplementary information file, an array of electrodes was formed on an OET bottom plate, each insulated from the a-Si:H layer below, and each pair separated by a
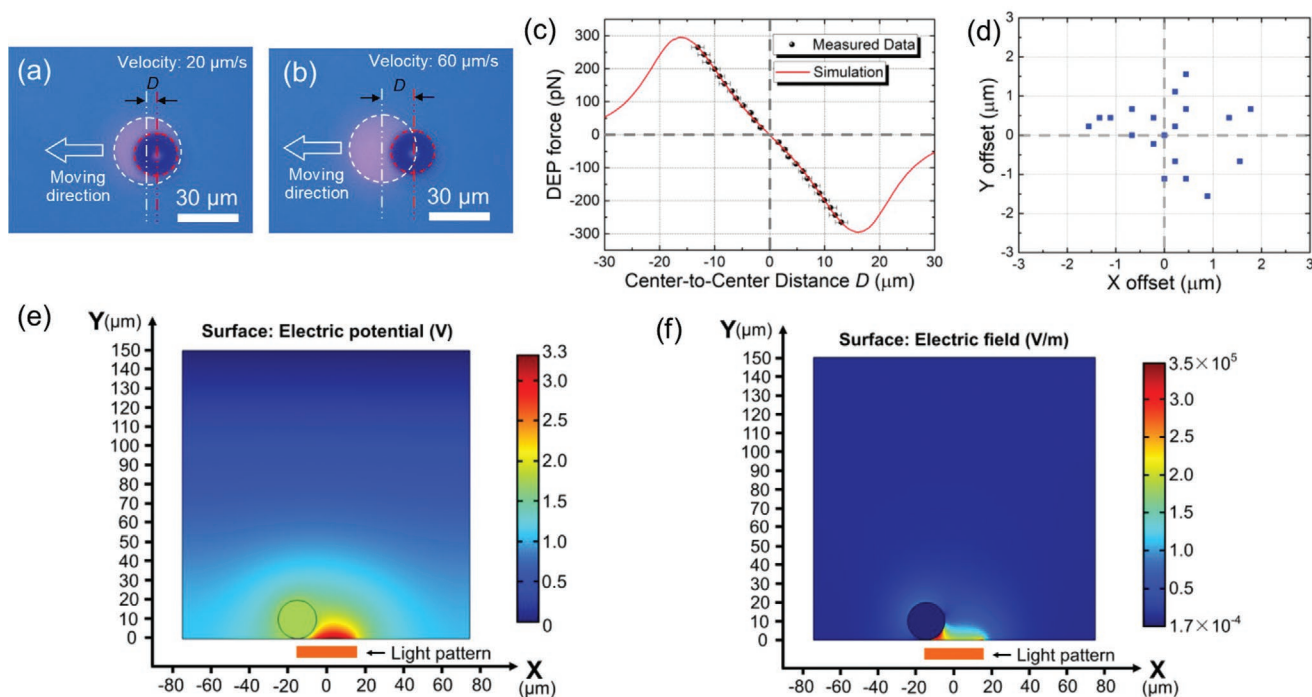

Figure 5. OET manipulation of solder beads. Bright-field microscope images (frames from Movie S4 in the Supporting Information) illustrating the translation of a 20 µm diameter solder bead at a) 20 µm s⁻¹, and b) 60 µm s⁻¹ using a 30 µm diameter circular light pattern (from Movie S4 in the Supporting Information) in concentrated PEGDA diluted 1:4 in DI water. The white arrow indicates the direction of movement and the white and red dashed outlines indicate the positions of the light pattern and the solder bead, respectively. c) Measured trap profile (markers) and simulated trap profile (by Maxwell stress tensor, solid red line) for the conditions illustrated by (a) and (b). Error bars represent standard deviation for ten replicates per condition. d) Post-translation offsets measured for 18 solder beads in concentrated PEGDA diluted 1:4 in DI water before and after movement at least 30 µm. Simulated distribution of e) electric potential, and f) electric field in an OET device with a solder bead positioned at the left edge of the trap, formed by illuminating a 30 µm diameter circular light pattern (shaded in orange) onto the a-Si:H surface (at $Y = 0$). The simulated electric potential and field are indicated in heat maps (blue = low; red = high) and the solder bead is illustrated as a hollow black circle.
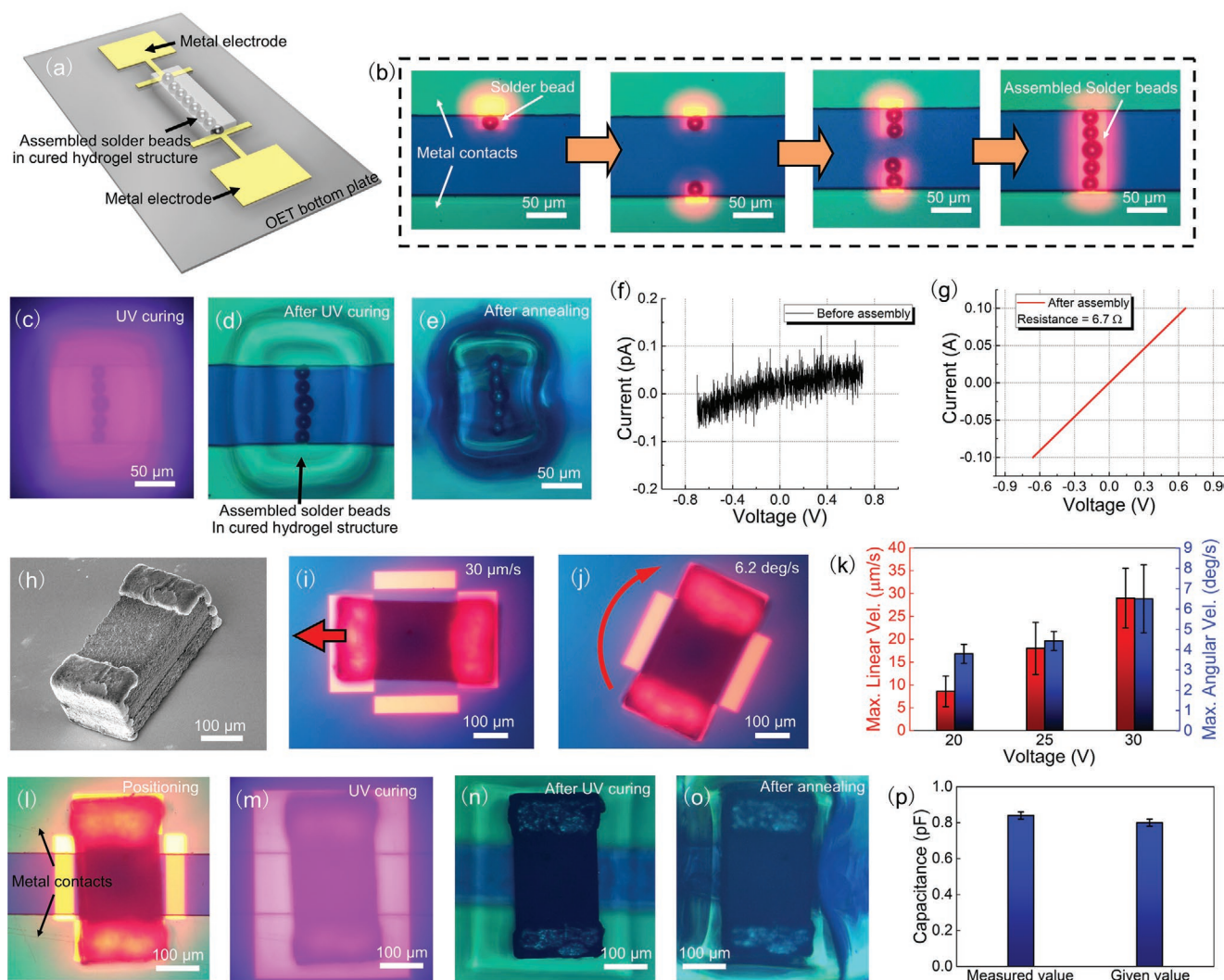
**ADVANCED
SCIENCE NEWS**

www.advancedsciencenews.com

NANO · MICRO
small

www.small-journal.com

Figure 6. Top-down assembly of microelectronic circuits and preservation via UV photopolymerization. a) Schematic of OET-assembled solder beads (gray) in cured hydrogel connecting two metal electrodes (yellow) on an OET bottom plate. b) Bright-field microscopy images (frames from Movie S5 in the Supporting Information, left-to-right), illustrating the process of using OET to manipulate five solder beads into position to bridge a gap between electrodes. Images of the assembled solder beads from b) while curing c), after curing d), and after annealing e). I–V measurements of metal contacts f) before and g) after being connected by an OET-assembled conductive trace (and then cured and annealed). h) SEM image of a microcapacitor. Bright-field microscope images (frames from Movie S6 in the Supporting Information), illustrating the process of using OET to i) move the capacitor at 30 µm s⁻¹, and j) rotate the capacitor at 6.2 rad s⁻¹, with red arrows indicating the direction of motion. k) Plot of maximum linear velocity (left axis, red) and angular velocity (right axis, blue) for OET-driven translation and rotation of microcapacitors as a function of bias voltage. Error bars represent standard deviation for five replicates. Bright-field microscopy images of illustrating a microcapacitor after positioning between two electrodes l), while curing m), after curing n), and after annealing o). Capacitance measurements of electrodes p) before and after being connected by an OET-positioned capacitor (and then cured and annealed). Error bars for measured value represent standard deviation for 3 replicates (different capacitors/electrode pairs); error bars for the given value represent the tolerance provided by the manufacturer. In bright field images, the projected light patterns are red, the electrodes appear green, the space between them appears blue, and manipulations were in conc. PEGDA diluted 1:4 in DI water.

gap (in space) of 100 µm (Figure S5, Supporting Information). **Figure 6**a shows the goal—a line of solder beads connecting two formerly isolated electrodes. As illustrated in Movie S5 (Supporting Information) and Figure 6b, it is straightforward to use OET to align the beads in top-down mode, in which individual particles are picked and placed precisely, as needed. As illustrated in Figure 6c–e, the pattern can be made permanent and conductive by photocuring, drying, and annealing, and finally, as shown in Figure 6f,g, the resistances between the isolated metal contacts before and after assembling the solder

beads (with annealing) were measured to be around 10^{13} Ω (noise floor) and 6.7 Ω, respectively. These results demonstrate the potential for using OET manipulation to assemble, interconnect, and create microelectronics that are permanently assembled in a UV-cured polymer.

As a final step toward microcircuit assembly, we explored the capacity of the technique to position, affix, and immobilize a thin-film microcapacitor to form a capacitive circuit. As shown in Figure 6h, the unit tested here is 400 µm × 200 µm × 170 µm ($l \times w \times h$), and comprises a dielectric region flanked by

**ADVANCED
SCIENCE NEWS**
www.advancedsciencenews.com

NANO · MICRO
small
www.small-journal.com

conductive terminals bearing solder on each side. As shown in Movie S6 (Supporting Information), clip 1, in initial tests with a simple, stationary rectangular light pattern, the capacitor was found to oscillate from side to side. We hypothesize that this interesting behavior arises from the Janus-like nature of the particle, which likely experiences positive DEP on its conductive ends and negative DEP in the center. As shown in Move S6 in the Supporting Information (clips 2 and 3) and Figure 6i,j, stable control was achieved over the microcapacitor by projecting a custom "positive/negative cage" pattern into the chamber. To the best of our knowledge, this is the largest (0.0136 mm^3) and heaviest object (0.04 mg) that has been reported to be controllable by any optical micromanipulation technique previously. The maximum linear velocity and angular velocity of the microcapacitor when manipulated in this manner were found to scale with the applied bias voltage (Figure 6k), similar to the objects that experience only positive or negative DEP force.[34] As illustrated in Figure 6l–o, the techniques described here can be used to position a microcapacitor such that it bridges isolated electrodes in a microelectronic circuit, and that this can be made permanent and functional by photocuring, drying and annealing. Finally, as shown in Figure 6p, the capacitance of such structures was measured to be around 0.86 pF, close to the value given by the manufacturer (0.80 pF). As far as we are aware, this is the first report of the assembly of a microcapacitive circuit using optical micromanipulation techniques, which suggests utility for a wide range of applications in the future.

3. Conclusion

In this work, we demonstrated how OET can be used to assemble nano/micromaterials to form tailored, artificial microstructures, which can then be immobilized/preserved in photocurable hydrogels via in situ photopolymerization. The system is easy to use with a user-friendly computer interface. We demonstrated that carbon/silver nanoparticles, graphene nanoplatelets and polystyrene microparticles can be assembled to form TMPs in cured hydrogel structures, which can then be transferred to alternate substrates. In addition, the method was demonstrated to be useful for forming conductive structures to bridge isolated metal electrodes, and assembly of capacitive components. This work demonstrates great potential for using OET and in situ photopolymerization for assembly and building microstructures and microelectronics on demand.

4. Experimental Section

Instrumentation and Devices: The instrument used in this work is similar to one reported previously,[34] featuring a projector interfaced to an upright microscope (Leica DM 2000 with motorized stage Märzhäuser Scan Plus 100×100). In this work, the projector is a Polygon DMD Illuminator (Mightex Inc.) with two independently controlled LED light sources at 380 nm (UV) and 620 nm (red), respectively, with intensities and other parameters given in the supplementary information. The OET device used in this work comprised a 30 μL fluidic chamber sandwiched in between a top and a bottom plate using 150 μm thick double sided tape (3M 9965). Each plate was formed from a glass slide coated with 200 nm thick ITO, with the bottom plate featuring

an additional photoconductive layer of 1 μm thick a-Si:H, deposited by plasma enhanced chemical vapor deposition (PECVD)[28]. In some cases (e.g., Figure 6), metal electrodes were fabricated on top of the a-Si:H layer of the bottom plate (see the Supporting Information and Figure S5 for fabrication details). OET devices were driven by applying a sine-wave bias between the top and bottom plates. For most experiments, the bias was 15 V$_{pp}$ at 20 kHz; for those involving the manipulation of microcapacitors, the bias varied, but typically was 25 V$_{pp}$ at 20 kHz.

Preparation of Hydrogel Solution for Photopolymerization: A hydrogel prepolymer solution was prepared by dissolving PEGDA (Sigma-Aldrich, 455008) and poly(ethylene glycol) (PEG, Sigma-Aldrich, 202398) into deionized (DI) water containing 0.05% (v/v) Tween 20 (Sigma-Aldrich, P2287). The composition was 30% (v/v) PEGDA, 40% (v/v) PEG, and 30% (v/v) DI water (with Tween 20). Finally, 0.5% (w/v) diphenyl(2,4,6-trimethylbenzoyl)-phosphine oxide (TPO, Sigma-Aldrich, 906808) was dissolved in the hydrogel solution, which functions as photoinitiator to trigger the UV-activatable crosslinking reaction. This mixture was known as the "concentrated PEGDA solution," which was diluted in different ratios in DI water containing 0.05% (v/v) Tween 20 for most applications. The conductivity and viscosity of a 1:4 dilution of concentrated PEGDA was measured to be 1.8×10^{-2} S m^{-1} and 7.6×10^{-3} Pa s, respectively.

Measurement of Curing Time and Curing Percentage for Solutions with Different Ratios of Concentrated PEGDA to DI Water: In each experiment, a solid rectangular light pattern (900 μm × 550 μm) was projected into an OET device filled with a solution of PEGDA. The cured region could be identified manually by a change in contrast, and UV illumination was continuously applied for a duration of t_{ill} s, and turned off when the first of the following conditions were met: (1) the cured hydrogel structure completely covered the illuminated region or (2) the cured region did not show an observable change or expansion for 90 s. The curing time for each condition was then recorded as t_{ill} for (1) and $t_{ill} - 90$ s for (2). After curing, the percentage of the cured area (compared to the area of the UV light pattern) was calculated using ToupView software (ToupTek Photonics). The curing time and curing percentage were measured five times per condition on five different devices. When following the conditions indicated above (which ensured that the chamber was not overexposed), the fluid in the remainder of the chamber was not affected, such that additional photopolymerized structures could be formed.

Preparation of Samples for OET Manipulation: Two kinds of polystyrene microspheres (with nominal average diameters provided by the supplier, Polysciences) were used in this work: 10 μm dia. plain microbeads (Polysciences, 17136), and 6 μm dia. red fluorescent microbeads (Polysciences, 19111), which were provided by the supplier as aqueous suspensions and then centrifuged and resuspended at 0.1 to 1×10^7 particles mL^{-1} in DI water containing 0.05% (v/v) Tween 20. Carbon nanoparticles (Sigma-Aldrich, 633100), silver nanoparticles (Sigma-Aldrich, 576832), graphene nanoplatelets (Sigma-Aldrich, 799084), and solder microbeads (15–25 μm spheres of Sn$_{96.5}$Ag$_3$Cu$_{0.5}$ from Industrie des Poudres Sphériques) were provided in powder form by the supplier. Nanomaterials (carbon, silver, and graphene) were suspended (seprately) at 30 mM, and solider microbeads were suspended (separately) at 0.1 to 1×10^6 particles mL^{-1} in DI water containing 0.05% (v/v) Tween 20. Prior to each experiment, the relevant suspension of nano/micromaterials was sonicated using an ultrasonic probe (Sonics and Materials Inc., VCX 130) for 5 min, and then it was mixed at various ratios (most often 4:1) with concentrated PEGDA solution. Finally, in each microcapacitor experiment, 0.80 pF thin-film capacitors (C005YK0R8PBSTR, AVX Corporation) were suspended in in DI water containing 0.05% (v/v) Tween 20 diluted 4:1 with concentrated PEGDA.

Bottom-Up TMP Assembly, Harvesting, and Transfer: 30 μL of a homogenous suspension of particles in diluted PEGDA solution was loaded into the OET device. The desired red-light pattern was projected into the system until particle assembly was observed (typically within 60 s). The OET device was submerged vertically in a beaker in DI water solution for 2 min. The OET device was then removed and placed in an oven at 50 °C for 3 min. After drying, the OET top plate was gently removed, leaving the cured hydrogel microstructure with the assembled TMP on the surface of the OET bottom plate. TMPs were then

transferred to other destination substrates using the method reported previously.[29] Harvested, transferred TMPs were characterized by bright-field microscopy or scanning electron microscopy (see the Supporting Information for details for the latter). Some fluorescent TMPs were characterized by fluorescence microscopy.

Top-Down Particle Manipulation Experiments: For experiments with polystyrene microparticles or solder microbeads, 20 µL of the solution without microparticles was pipetted into the chamber of the OET device, followed by another injection of 10 µL of the same solution with microparticles. This arrangement allows for a region of the chamber to be free of microparticles, providing space for manipulation. For polystyrene particles, a doughnut-shaped red-light pattern (with inner and outer diameter 100 µm and 160 µm, respectively) was used to select and isolate an individual particle as in Figure 2a,b, The particle was moved by keeping the light pattern stationary while translating the motorized microscope stage (and OET device) at a known velocity. To measure maximum velocity, the translational velocity of the motorized stage was gradually increased until the DEP force exerted on the particle could no longer match the viscous drag force such that the particle escaped from the light pattern, as described previously[44]. The highest velocity that allowed successful bead transport was defined as its maximum moving velocity. For each condition evaluated, this property was measured for 5 movable particles on 5 different devices. In each such experiment, 20 particles (on a given device) were also tested for a "yes" or "no" measurement of "movability" (at 1 µm s^{-1}). The percentage of movable particles was calculated from the 20 tests, which were repeated five times on five different devices. For solder microbeads, a red-light circular light pattern (with 30 µm diameter) was used to select and isolate an individual particle as in Figure 5a,b. Each particle's radius was measured and was moved at a given translational velocity (by moving the stage, as above), recording the center-to-center distance D between the light pattern and the particle. D was measured for 10 particles per velocity and was used to estimate the DEP force experienced by the particle according to Equation (1). Since the solder beads have a density of 8 g cm^{-3}, and the DEP force also pulls them to the bottom of the OET chamber, Faxen's correction was applied to the estimate, as described previously for other materials.[45,46] To measure the positioning accuracy of solder beads, in each experiment, a bead was initially confined in a 30 µm diameter circular (red-light) OET trap. The position of the bead center relative to the trap center (in *X*- and *Y*-dimensions) was estimated using the microscope's image analyzing software (ToupView 3.7). The trap was then moved to a destination position (with the *X*- and *Y*-coordinates of the destination selected randomly to be between 30 and 500 µm away from the initial trap-center coordinates) at 15 µm s^{-1}, after which the position of the bead center relative to the trap center was estimated again. The differences between the initial and final relative positions were then reported as "post-translation offsets." This process was repeated for 18 different beads. Finally, for each experiment with microcapacitors, a 30 µL aliquot of a 1:4 dilution of concentrated PEGDA containing a single microcapacitor was loaded into a device. A red-light pattern dubbed the "positive/negative cage" comprising four solid bars (two thick 250 µm × 110 µm bars separated by 210 µm arranged perpendicularly to two thin 210 µm × 45 µm bars separated by 270 µm) was projected into the OET device. This pattern was translated (by moving the microscope stage) and rotated (by rotating the projected image) until the large bars covered the solder-coated edges of the capacitor, and the thin bars were just outside of the non-coated edges of the capacitor. Maximum linear velocity and angular velocity for microcapacitors were determined using methods described previously for other particles.[34]

Top-Down Assembly of Microelectronic Circuit Components: Microelectronic circuits were formed by loading either a suspension of solder beads or a single microcapacitor a 1:4 dilution of concentrated PEGDA into modified OET devices bearing isolated electrodes with 100 µm gap (fabricated as described in the Supporting Information and Figure S5). For solder beads, rectangular red-light patterns (30 µm × 20 µm or 20 µm × 25 µm) were used to collect and position solder beads between a pair of electrodes, one-by-one, by manipulating the

microscope stage relative to the projected pattern. As each solder bead was added to the structure, the light pattern used to position it was kept "on" and immobile, holding the structure in place while the next solder bead was collected. The structure was then cured as described above, and the device was submerged vertically in a beaker in DI water solution for 2 min and then dried in an oven (50 °C for 3 min). Finally, the solder was annealed on a hotplate at 220 °C for 2 min. The current–voltage (*I–V*) characteristics of pairs of electrodes in devices before and after forming solder-bead electrical traces were determined using a semiconductor device analyzer/probe station (Keithley 4200 SCS). For microcapacitor manipulation, the positive/negative cage pattern was projected into the device, and a combination of translation and rotation steps (described above) was used to position the capacitor such that it bridged a pair of isolated electrodes. The circuit was then cured, dried and annealed as described above for the solder beads. The capacitance of pairs of electrodes on three different devices bridged by three different capacitors was measured using a capacitance meter (Model 3000, GLK Instruments).

Supporting Information

Supporting Information is available from the Wiley Online Library or from the author.

Conflict of Interest

The authors declare no conflict of interest.

Author Contributions

S.Z. and W.L. conceived the idea and carried out the OET experiments. S.Z and M.E. built the experimental setup. W.L. and J.P. prepared and optimized the sol-form PEGDA solution. Y.C. and Y.Z. deposited the a-Si:H materials. S.Z., M.E., and M.S. fabricated the OET devices. Y.Z., W.D., and T.W. performed the IV measurement. S.Z. and A.R.W. wrote the manuscript. All authors discussed the results and commented on the manuscript. Y.S., N.P.K., S.L.N. and A.R.W. coordinated and supervised the project.

Data Availability Statement

Raw data are available from the corresponding author upon request.

Keywords

 [1] A. Carlson, A. M. Bowen, Y. Huang, R. G. Nuzzo, J. A. Rogers, *Adv. Mater.* **2012**, *24*, 5284.

 [2] M. A. Meitl, Z. T. Zhu, V. Kumar, K. J. Lee, X. Feng, Y. Y. Huang, I. Adesida, R. G. Nuzzo, J. A. Rogers, *Nat. Mater.* **2006**, *5*, 33.

 [3] T. H. Kim, K. S. Cho, E. K. Lee, S. J. Lee, J. Chae, J. W. Kim, D. H. Kim, J. Y. Kwon, G. Amaratunga, S. Y. Lee, B. L. Choi, *Nat. Photonics* **2011**, *5*, 176.

 [4] Y. Zhang, B. K. Chen, X. Y. Liu, Y. Sun, *IEEE. Trans. Robot.* **2010**, *26*, 200.

 [5] B. K. Chen, Y. Zhang, Y. Sun, *J. Microelectromech. Syst.* **2009**, *18*, 652.

 [6] D. Jevtics, A. Hurtado, B. Guilhabert, J. McPhillimy, G. Cantarella, Q. Gao, H. H. Tan, C. Jagadish, M. J. Strain, M. D. Dawson, *Nano Lett.* **2017**, *17*, 5990.

 [7] B. Guilhabert, A. Hurtado, D. Jevtics, Q. Gao, H. H. Tan, C. Jagadish, M. D. Dawson, *ACS Nano* **2016**, *10*, 3951.

 [8] A. J. Trindade, B. Guilhabert, E. Y. Xie, R. Ferreira, J. J. McKendry, D. Zhu, N. Laurand, E. Gu, D. J. Wallis, I. M. Watson, C. J. Humphreys, *Opt. Exp.* **2015**, *23*, 9329.

 [9] J. E. Melzer, E. McLeod, *Nanophotonics* **2020**, *9*, 1373.

[10] A. Ashkin, J. M. Dziedzic, T. Yamane, *Nature* **1987**, *330*, 769.

[11] D. G. Grier, *Nature* **2003**, *424*, 810.

[12] K. Dholakia, T. Čižmár, *Nat. Photonics* **2011**, *5*, 335.

[13] M. Daly, M. Sergides, S. N. Chormaic, *Laser Photonics Rev.* **2015**, *9*, 309.

[14] L. Lin, X. Peng, X. Wei, Z. Mao, C. Xie, Y. Zheng, *ACS Nano* **2017**, *11*, 3147.

[15] L. Lin, J. Zhang, X. Peng, Z. Wu, A. C. H. Coughlan, Z. Mao, M. A. Bevan, Y. Zheng, *Sci. Adv.* **2017**, *3*, 1700458.

[16] L. Lin, M. Wang, X. Peng, E. N. Lissek, Z. Mao, L. Scarabelli, E. Adkins, S. Coskun, U. Sahin, H. E. Unalan, B. A. Korgel, L. M. Liz-Marzán, E. L. Florin, Y. Zheng, *Nat. Photonics* **2018**, *12*, 195.

[17] M. Jubera, I. Elvira, A. García-Cabañes, J. L. Bella, M. Carrascosa, *Appl. Phys. Lett.* **2016**, *108*, 023703.

[18] M. Carrascosa, A. García-Cabañes, M. Jubera, J. B. Ramiro, F. Agulló-López, *Appl. Phys. Rev.* **2015**, *2*, 040605.

[19] I. Elvira, J. F. Muñoz-Martínez, Á. Barroso, C. Denz, J. B. Ramiro, A. García-Cabañes, F. Agulló-López, M. Carrascosa, *Opt. Lett.* **2018**, *43*, 30.

[20] A. Puerto, A. Méndez, L. Arizmendi, A. García-Cabañes, M. Carrascosa, *Phys. Rev. Appl.* **2020**, *14*, 024046.

[21] M. C. Wu, *Nat. Photonics* **2011**, *5*, 322.

[22] P. Y. Chiou, A. T. Ohta, M. C. Wu, *Nature* **2005**, *436*, 370.

[23] H. Hwang, J. K. Park, *Lab Chip* **2011**, *11*, 33.

[24] W. Liang, L. Liu, J. Wang, X. Yang, Y. Wang, W. J. Li, W. Yang, *Micromachines* **2020**, *11*, 78.

[25] Y. Huang, Z. Liang, M. Alsoraya, J. Guo, D. E. Fan, *Adv. Intell. Syst.* **2020**, *2*, 1900127.

[26] M. B. Lim, R. G. Felsted, X. Zhou, B. E. Smith, P. J. Pauzauskie, *Appl. Phys. Lett.* **2018**, *113*, 031106.

[27] M. B. Lim, J. L. Hanson, L. Vandsburger, P. B. Roder, X. Zhou, B. E. Smith, F. S. Ohuchi, P. J. Pauzauskie, *J. Mater. Chem. A* **2018**, *6*, 5644.

[28] S. Zhang, N. Shakiba, Y. Chen, Y. Zhang, P. Tian, J. Singh, M. D. Chamberlain, M. Satkauskas, A. G. Flood, N. P. Kherani, S. Yu, P. W. Zandstra, A. R. Wheeler, *Small* **2018**, *14*, 1803342.

[29] S. Zhang, Y. Zhai, R. Peng, M. Shayegannia, A. G. Flood, J. Qu, X. Liu, N. P. Kherani, A. R. Wheeler, *Adv. Opt. Mater.* **2019**, *7*, 1900669.

[30] W. Liang, L. Liu, S. H. Lai, Y. Wang, G. B. Lee, W. J. Li, *Opt. Mater. Express* **2014**, *4*, 2368.

[31] S. Liang, Y. Cao, Y. Dai, F. Wang, X. Bai, B. Song, C. Zhang, C. Gan, F. Arai, L. Feng, *Micromachines* **2021**, *12*, 271.

[32] J. Juvert, S. Zhang, I. Eddie, C. J. Mitchell, G. T. Reed, J. S. Wilkinson, A. Kelly, S. L. Neale, *Opt. Exp.* **2016**, *24*, 18163.

[33] S. Zhang, J. Juvert, J. M. Cooper, S. L. Neale, *Sci. Rep.* **2016**, *6*, 32840.

[34] S. Zhang, E. Y. Scott, J. Singh, Y. Chen, Y. Zhang, M. Elsayed, M. D. Chamberlain, N. Shakiba, K. Adams, S. Yu, C. M. Morshead, P. W. Zandstra, A. R. Wheeler, *Proc. Natl. Acad. Sci. U. S. A.* **2019**, *116*, 14823.

[35] S. Zhang, Y. Liu, Y. Qian, W. Li, J. Juvert, P. Tian, J. C. Navarro, A. W. Clark, E. Gu, M. D. Dawson, J. M. Cooper, S. L. Neale, *Opt. Exp.* **2017**, *25*, 28838.

[36] R. Pethig, *Biomicrofluidics* **2010**, *4*, 022811.

[37] S. Zhang, W. Li, M. Elsayed, P. Tian, A. W. Clark, A. R. Wheeler, S. L. Neale, *Opt. Lett.* **2019**, *44*, 4171.

[38] A. Jamshidi, P. J. Pauzauskie, P. J. Schuck, A. T. Ohta, P. Y. Chiou, J. Chou, P. Yang, M. C. Wu, *Nat. Photonics* **2008**, *2*, 86.

[39] Z. Chen, F. Nan, Z. Yan, *J. Phys. Chem. C* **2020**, *124*, 4215.

[40] X. Peng, J. Li, L. Lin, Y. Liu, Y. Zheng, *ACS Appl. Nano Mater.* **2018**, *1*, 3998.

[41] X. Zhou, Y. Hou, J. Lin, *AIP Adv.* **2015**, *5*, 030701.

[42] K. Salaita, S. W. Lee, X. Wang, L. Huang, T. M. Dellinger, C. Liu, C. A. Mirkin, *Small* **2005**, *1*, 940.

[43] P. Y. Chiou, Interactive Microparticle Manipulation Using OET [Video file], https://www.youtube.com/watch?v=_FkROvhVzCo&list =UUX6e2chk7w6xSDQLcdG1UKQ&index=19 (accessed: September 2019).

[44] S. Zhang, A. Nikitina, Y. Chen, Y. Zhang, L. Liu, A. G. Flood, J. Juvert, M. D. Chamberlain, N. P. Kherani, S. L. Neale, A. R. Wheeler, *Opt. Express* **2018**, *26*, 5300.

[45] S. L. Neale, M. Mazilu, J. I. Wilson, K. Dholakia, T. F. Krauss, *Opt. Express* **2007**, *15*, 12619.

[46] S. B. Huang, M. H. Wu, Y. H. Lin, C. H. Hsieh, C. L. Yang, H. C. Lin, C. P. Tseng, G. B. Lee, *Lab Chip* **2013**, *13*, 1371.

[47] S. Zhang, Y. Liu, J. Juvert, P. Tian, J. C. Navarro, J. M. Cooper, S. L. Neale, *Appl. Phys. Lett.* **2016**, *109*, 221110.

[48] X. Wang, X. B. Wang, P. R. C. Gascoyne, *J. Electrostat.* **1997**, *39*, 277.

[49] S. Kumar, P. J. Hesketh, *Sens. Actuators, B* **2012**, *161*, 1198.

[50] R. J. Barsotti, M. D. Vahey, R. Wartena, Y. M. C. J. Voldman, F. Stellacci, *Small* **2007**, *3*, 488.

[51] N. Liu, W. Liang, J. D. Mai, L. Liu, G. B. Lee, W. J. Li, *IEEE Trans. Nanotechnol.* **2014**, *13*, 245.

[52] Y. H. Lin, K. S. Ho, C. T. Yang, J. H. Wang, C. S. Lai, *Opt. Express* **2014**, *22*, 13811.